Nuclear Quantum Effects in Gas-Phase 2-Fluoroethanol

Electronic Supporting Information

Mrinal Arandhara and Sai G. Ramesh*
Department of Inorganic and Physical Chemistry, Indian Institute of Science, Bangalore 560012

TABLE S-1. Ab initio energies at the local minima and TS geometries of 2FE at various levels of theory. All energies are in cm^{-1}.

	G^+g^- G^-g^+	G^+t G^-t	Tt	Tg^+ Tg^-	G^+g^+ G^-g^-	Cc
MP2/aVDZ	0.0	717.3	767.6	830.8	901.4	2482.0
CCSD/aVDZ	0.0	715.4	702.6	776.9	885.6	2388.0
CCSD(T)/aVDZ//MP2/aVDZ	0.0	741.2	749.9	790.5	894.0	2345.1
CCSD(T)/aVDZ//CCSD/aVDZ	0.0	740.2	749.4	791.3	893.4	2347.0
MP2/aVTZ	0.0	685.6	755.6	813.6	861.0	2386.8
CCSD(T)/aVTZ//MP2/aVTZ	0.0	710.3	745.5	780.0	855.5	2253.7

TABLE S-2. Normal mode frequencies of 2FE at various stationary points. All frequencies are in cm^{-1}.

	G^+g^-	G^+t	Tt	Tg^+	G^+g^+	Cc
	63.58	72.2	180.0	178.9	65.2	0.0
	−58.02	−167.2	180.0	76.1	63.2	0.0
ω_1	155.2	158.7	115.5	133.4	151.2	i245.9
ω_2	315.4	199.4	213.9	261.2	240.0	226.7
ω_3	376.2	330.6	285.9	283.1	327.7	322.5
ω_4	518.6	498.9	472.3	467.7	514.0	617.4
ω_5	873.4	892.3	832.0	812.5	880.2	857.0
ω_6	907.8	917.0	1039.4	1056.3	906.3	907.8
ω_7	1061.0	1088.4	1085.6	1072.8	1067.2	1079.7
ω_8	1121.4	1107.5	1091.5	1102.1	1100.1	1136.8
ω_9	1137.5	1132.9	1176.0	1113.8	1143.4	1169.6
ω_{10}	1232.0	1243.2	1241.2	1225.4	1227.9	1279.7
ω_{11}	1280.9	1281.0	1245.3	1319.9	1311.2	1294.6
ω_{12}	1386.9	1327.2	1317.6	1356.1	1381.3	1304.5
ω_{13}	1411.3	1420.4	1391.2	1387.8	1415.3	1421.9
ω_{14}	1439.6	1471.8	1476.0	1446.0	1442.0	1458.2
ω_{15}	1510.1	1515.5	1540.3	1529.8	1506.0	1538.5
ω_{16}	1518.6	1517.5	1550.2	1541.5	1519.1	1563.5
ω_{17}	3065.2	3043.6	3062.7	3082.3	3047.0	3076.2
ω_{18}	3098.0	3093.4	3108.3	3091.8	3076.1	3116.8
ω_{19}	3145.5	3107.6	3115.5	3152.5	3135.7	3117.0
ω_{20}	3170.0	3163.2	3177.3	3174.6	3157.4	3184.1
ω_{21}	3825.4	3856.5	3858.7	3844.9	3837.0	3822.0

PES web link:
The model PES for 2FE used in this work may be found at this Github page:
`https://github.com/arandharamrinal/2FE`.

TABLE S-3. Root mean square errors for fits of optimal values of symmetrized internals S_j° on the reaction surface. Based on a given mode's symmetry (Table II), Eq. (4) or (5) was used. In all cases, $(M, N) = (8, 6)$ was used to obtain an accurate fit.

Bonds	RMSE (Å, $\times 10^{-5}$)	MAE	Angles	RMSE ($^\circ$, $\times 10^{-3}$)	MAE	Dihedrals	RMSE ($^\circ$, $\times 10^{-3}$)	MAE
S_1°	1.96	1.74	S_9°	3.52	2.77	S_{16}°	2.03	1.67
S_2°	0.72	0.59	S_{10}°	2.78	2.03	S_{17}°	1.68	1.19
S_3°	0.86	0.63	S_{11}°	1.20	1.01	S_{18}°	2.06	2.13
S_4°	0.18	0.15	S_{12}°	1.62	1.19	S_{19}°	2.26	1.33
S_5°	0.12	0.09	S_{13}°	2.17	1.73			
S_6°	0.15	0.14	S_{14}°	1.70	1.41			
S_7°	0.16	0.10	S_{15}°	2.33	1.82			
S_8°	0.81	0.56						

S-1. DEVELOPMENT OF THE DIPOLE MOMENT SURFACE FOR 2FE

A. DMS modelling

Towards the computation of infrared spectra for 2FE via path integral simulations, we have fitted a dipole moment surface of the form

$$\begin{aligned}\boldsymbol{\mu} &= \boldsymbol{\mu}_{rs} + \boldsymbol{\mu}_b \\ &= \sum_k q_{rs,k}(\phi_1, \phi_2)\boldsymbol{r}_k + \sum_k q_{b,k}(\delta\boldsymbol{S}|\phi_1, \phi_2)\boldsymbol{r}_k.\end{aligned} \tag{1}$$

The above partitioning of $\boldsymbol{\mu}$ into reaction surface and remainder components is carried out in the same manner as done for the potential (Eq. (1), main manuscript). As shown in an earlier work [2] , the dipole moment surface may be modelled through the set of scalar atomic charges ($q_k = q_{rs,k} + q_{b,k}$, where k is the atom number) that are functionally dependent on internal coordinates and atom positions ($\boldsymbol{r}_k$). Presently, we expand the charges in terms of the reaction surface modes (ϕ_1, ϕ_2) and other internals ($\boldsymbol{S}$) in a manner similar to terms in the potential.

The reaction surface atomic charges, $q_{rs,k}(\phi_1, \phi_2)$, are fitted to individual dihedral expansions. The reference values are taken as HLY charges obtained at the same geometries used for the modelling of V_{rs}. However, the charges on the CH hydrogen atoms do not have definite even/odd symmetry, just as their internals R also do not have definite symmetry. As shown in Table 2 (main manuscript), the difficulty is readily overcome by taking sum and difference combinations. We apply this to the atomic charges as well, which are then readily fitted to even/odd expansions in (ϕ_1, ϕ_2) as per Eqs. (4) and (5). With suitable expansion sizes, accurate fits for $\boldsymbol{\mu}_{rs}$ are obtained.

For the fitting of $\boldsymbol{\mu}_b$, we have limited the expansion of other internals $\boldsymbol{S}$ in $q_{b,k}$ to first order,

$$\begin{aligned}\boldsymbol{\mu}_b(\delta\boldsymbol{S}|\phi_1, \phi_2) &= \sum_k q_{b,k}(\delta\boldsymbol{S}|\phi_1, \phi_2)\boldsymbol{r}_k \\ &= \sum_k \sum_j f_{b,kj}(\phi_1, \phi_2)\delta s_j \boldsymbol{r}_k,\end{aligned} \tag{2}$$

since higher order expansions leads to a strong increase in the number of parameters to be determined. The $f_{b,kj}$ are essentially the derivatives of the first $q_{b,k}$ along various dimensionless internals, s_j. Although we first attempted to use numerical derivatives of HLY charges, these were found to have discontinuities in (ϕ_1, ϕ_2) space. Instead, we have directly fitted the residual dipole function $\boldsymbol{\mu}_b^{ab} = \boldsymbol{\mu} - \boldsymbol{\mu}_{rs}^{ab}$, where the $\boldsymbol{\mu}_{rs}^{ab}$ is the reaction surface dipole function using the ab initio rather than fitted charges, as follows. (1) The residual $\boldsymbol{\mu}_b^{ab}$ is determined at displacements of ± 0.03 Å and ± 0.04 Å for bonds and $\pm 1.5^\circ$ and $\pm 2.0^\circ$ for angles and dihedrals from each of the reaction surface points used for $\boldsymbol{\mu}_{rs}$. (2) The molecular frame is fixed by choosing the CC bond axis as $\hat{x}$ and using the C-C-O plane to define the xy plane. All geometries and hence dipole components are rotated to this frame. (3) Like the $q_{rs,k}$ for the H atoms, the corresponding charges $q_{b,k}$ are neither even nor odd functions of (ϕ_1, ϕ_2). By taking sum and difference combinations of the charges and also Cartesian coordinates of CH hydrogen atoms, the equation is symmetrized. Consequently,

TABLE S-4. Errors in fitted atomic charges (in a.u.) at the 294 (ϕ_1, ϕ_2) geometries. Fits are carried out with (M_{max}, N_{max}) = (10,8).

Atom	MAE ($\times 10^{-3}$)	RMSE ($\times 10^{-3}$)
C_1	2.56	3.58
C_2	2.43	3.60
O_3	0.49	0.65
F_4	0.54	0.73
H_5	0.80	1.14
H_6	0.79	1.12
H_7	0.82	1.15
H_8	0.78	1.07
H_9	0.27	0.33

TABLE S-5. Comparising of the fitted $\boldsymbol{\mu}_{rs}$ to the ab initio dipole moment on the dihedral surface. All quantities are in a.u.

	MAE ($\times 10^{-4}$)	RMSE ($\times 10^{-4}$)
μ_x	0.629	7.818
μ_y	1.623	2.006
μ_z	1.792	2.205

TABLE S-6. Comparison of the dipole moments at geometries displaced from the dihedral surface (see Sec. S-1 A). Large displacements refer to ±0.03 and ±0.04 Å in bonds and ±1.5° and ±2.0° in angles and dihedrals, while small displacements are ±0.002 Å and ±0.004 Å in bonds and ±0.1° and ±0.2° in angles and dihedrals. All errors are reported in a.u.

	MAE ($\times 10^{-4}$)			RMSE($\times 10^{-4}$)		
	$\Delta\mu_x$	$\Delta\mu_y$	$\Delta\mu_z$	$\Delta\mu_x$	$\Delta\mu_y$	$\Delta\mu_z$
Small displ	0.653	1.642	1.819	8.255	2.033	2.245
Large displ	1.322	2.811	3.215	3.125	4.195	5.214
Overall	0.988	2.227	2.517	2.285	3.297	4.015

the modified $f_{b,kj}$ expansion coefficients are even/odd functions in (ϕ_1, ϕ_2). (4) The expansion coefficients are also constrained by a charge neutrality condition, $\sum_k q_{b,k} = 0$. Note that such a restraint is already present in the HLY charges used to fit the $q_{rs,k}$. Using all the geometries discussed above, a system of linear equations[2] is prepared including the dihedral even/odd expansions as appropriate, and solved using the singular value decomposition (SVD) method from the Numpy package.[3] With appropriate dihedral expansion (M_{max}, N_{max}) sizes, accurate $\boldsymbol{\mu}_b$ fits are obtained.

B. DMS fits

Table S-4 shows the quality of the fit to the atomic charges for 2FE using HLY charges at 294 reaction surface points. The fits used $(M_{max}, N_{max}) = (10, 8)$. Using the fitted charges, the dipole moments on the reaction surface are compared with ab initio dipole moments componentwise in Table S-5. Finally, Table S-6 provides a comparison of the $\boldsymbol{\mu}_b$ part of the dipole expansion at the displaced geometries from the reaction surface (see Sec. S-1 A). Overall, the fits are found to be satisfactory.

S-2. PREPARATION OF THE SET OF TEST DATA POINTS

To measure the quality of the full dimensional PES, a test set of ab initio points was prepared with the following approach. From long PIMD simulations at 300 K with the potential truncated up to quartic terms, geometries of selected beads (every 16th) were sampled at 0.5 ps intervals. The sample points were mainly in the G^+g^- basis, but a small fraction were also from the G^+t and G^+g^+ regions. The sample points were filtered based on proximity. To this end, vectors composed of bond distances, bond angles and dihedrals are constructed for each geometry. From these, magnitudes of difference vectors between different geometries was calculated. Denoting these as l_b, l_a and l_d for a pair of geometries, it was ensured that at least two of the following criteria were satisfied: $l_b > 0.2$ Å, $l_b > 5^\circ$ and $l_d > 15^\circ$. A total of 1077 sample points were selected in this manner.

In order to sample points at other minima that are not accessed by PIMD, we have employed a sampling approach due to Brown[1] that is based on the quantum harmonic distribution (QHD). At each minimum of 2FE, the quantity $d(\tilde{\nu}_i, A) = h/(8\pi^2 c\tilde{\nu}_i)\coth(1/2A)$, where c is the speed of light, provides the variance for ith mode with frequency $\tilde{\nu}_i$ (in cm^{-1}). If $A = k_B T/hc\tilde{\nu}_i$, the exact QHD is obtained. However, A is treated as a dimensionless parameter here. The variances along all modes at a given minimum are used in a multidimensional Gaussian distribution to obtain random displacements in all normal modes, thereby generating sample geometries. By varying A, the spread of the distribution can be controlled. As shown by Brown [1], using A instead of temperature T has two related advantages. First, the sampling of low frequency modes is on a par with that for high frequency modes. Second, to generate sufficiently displaced high frequency modes, high T needs to be used. But this generates overly distorted geometries in low frequency modes. Such a problem is avoided by using suitable values of A instead. Following Brown, we have used $A = 0.5$, 1 and 2, and obtained geometries at the Tt, Tg^+ and G^+g^+. The selected geometries are such that (1) no internal is excessively displaced; geometries were discarded if $|R_i - \langle R_i\rangle| > 1.5\sigma(R_i)$, where the mean $\langle R_i\rangle$ and standard deviation $\sigma(R_i)$ were estimated from the PIMD simulation with the quartic potential, and (2) the chosen points satisfied the same geometric non-proximity criteria as used for the PIMD sampling. A total of 4500 points (500 points per A value per minimum) were selected in this manner.

Additional points were sampled to cover other regions of the (ϕ_1, ϕ_2) landscape away from the minima and not already covered by the PIMD sampling. For this, we took samples of points in selected regions from the umbrella sampling simulations along ϕ_1 amounting to 1402 points. From the last 3 ns of the classical 300 K WT-metaD simulations, an additional 500 points were sampled. In the selection of these points, it was ensured that the points are sufficiently apart from each other using the bond distance, angle and dihedral criteria discussed above.

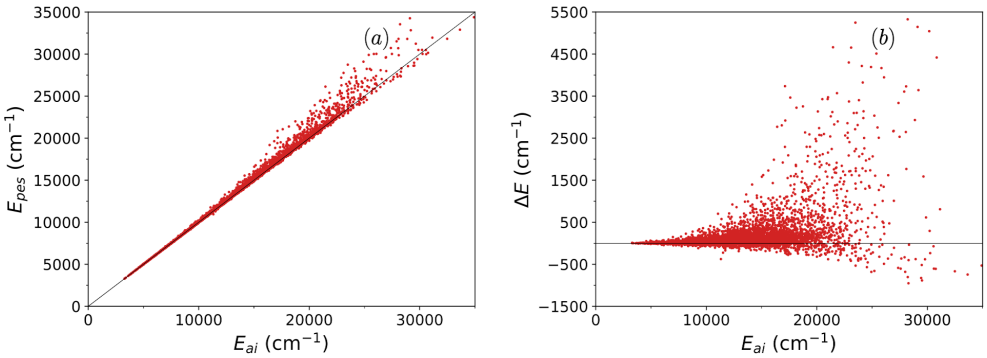

FIG. S-1. Comparison of abinitio MP2/aVTZ energies with the PES for 2FE truncated to quartic terms in V_b. The plots indicate large deviations at high energies, indicating the importance of including the higher order terms in the PES.

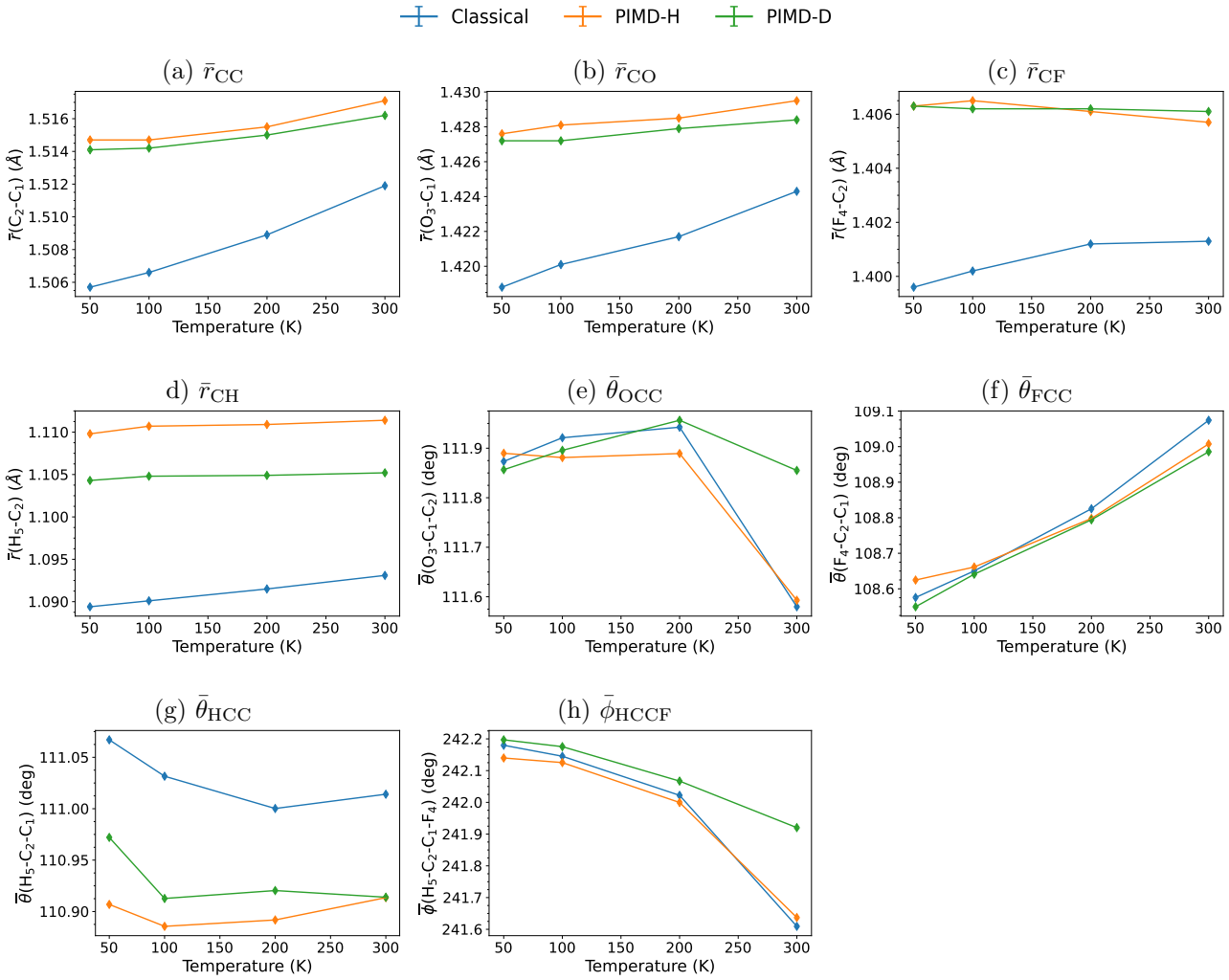

FIG. S-2. Averages of selected internals obtained from classical and PIMD simulations at various temperatures

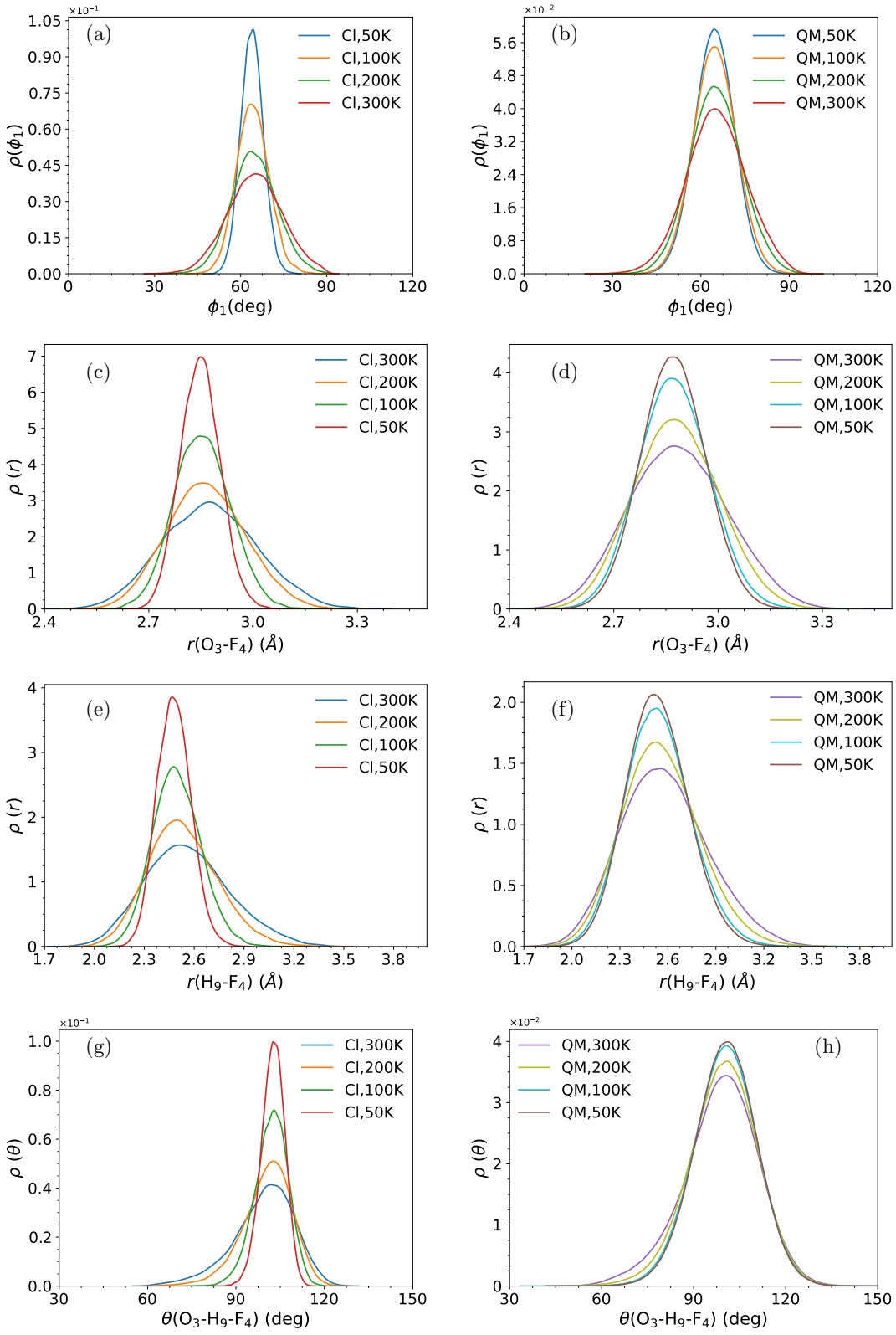

FIG. S-3. Classical and PIMD distributions of (a, b) ϕ_1, the (c, d) OF and (e, f) HF distances and (g, h) the HOF angle as a function of temperature for geometries restricted to the global minima. For this analysis, G^+g^- and G^-g^+ data were suitably combined; while the ϕ_1 value from the latter was mapped to the former basin, the other internals are invariant to dihedral mapping.

TABLE S-7. **Umbrella sampling parameters.** Bias form: $V_{umb}(\phi_1) = \frac{1}{2}K_{umb}(\phi_1 - \phi_1^\circ)^2$.

(1) 50 K simulations: Path integral umbrella sampling parameters along ϕ_1 are given in the table below. The centres of the umbrella potential ϕ_1°), corresponding force constant K, and length of simulation T_{sim} are shown. Note that 50 K classical simulations with umbrella sampling were also performed, but the resulting FES was not converged due to insufficient configuration sampling in the $\phi_1 = 120^\circ$ region despite different choices of K_{umb} attempted in that region. However, the estimated FES essentially overlaps with the 300 K classical FES up to about 100°

(2) 300 K simulations: Foth PIMD and classical simulations, the same ϕ_1° as given in the table are used with a fixed force constant $K_{umb} = 500$ kJ mol^{-1} rad^{-2}. All simulations were 200 ps long.

In all cases (50 K and 300 K) the first 10 ps are discarded as equilibration.

50 K, PIMD

ϕ_1°	T_{sim}	K_{umb}	ϕ_1°	T_{sim}	K_{umb}	ϕ_1°	T_{sim}	K_{umb}
0	400	200	60	200	500	120	500	200
5	400	200	65	200	500	125	500	200
10	400	200	70	200	500	130	500	200
15	400	200	75	200	500	135	500	200
20	400	200	80	200	500	140	500	200
25	400	200	85	200	500	145	500	200
30	400	200	90	200	500	150	500	200
35	400	200	95	200	500	155	500	200
40	200	500	100	500	200	160	500	200
45	200	500	105	500	200	165	500	200
50	200	500	110	500	200	170	500	200
55	200	500	115	500	200	175	500	200
						180	500	200

Units: ϕ_1° (deg), T_{sim} (ps), K (kJ mol^{-1} rad^{-2})

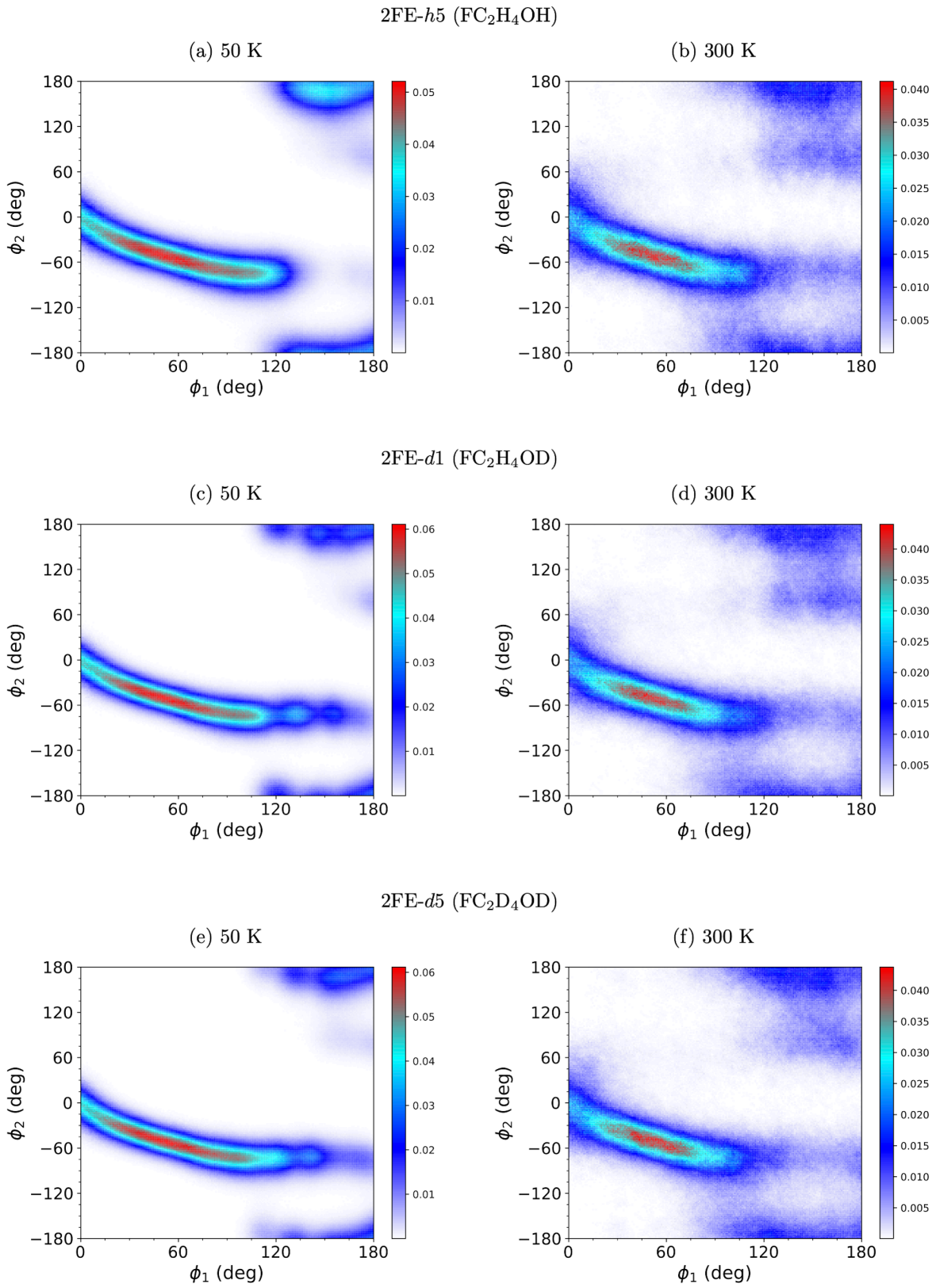

FIG. S-4. Distribution of centroid (ϕ_1, ϕ_2) values obtained via umbrella sampling simulations along ϕ_1 at both 50 K and 300 K. Plots are provided for 2FE-$h5$ (a, b), 2FE-$d1$ (c, d) and 2FE-$d5$ (e,f).

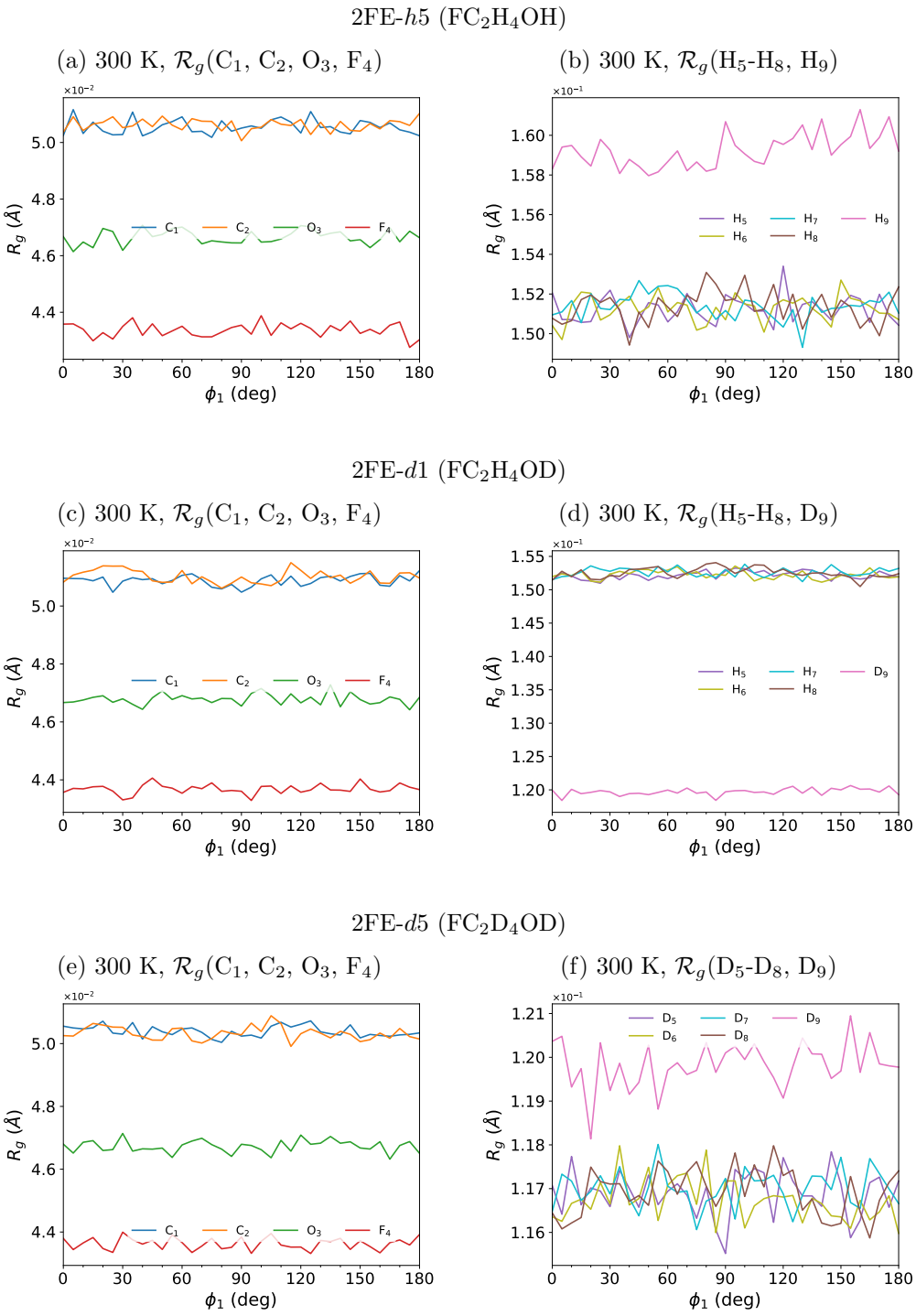

FIG. S-5. Radii of gyration, $\mathcal{R}_g$, for various atoms of 2FE from umbrella sampling simulations at 300 K as a function of the FCCO dihedral (ϕ_1). The top, middle and bottom rows provide the trends for 2FE-*h*5, 2FE-*d*1 and 2FE-*d*5, respectively. The plots in the left column (a, c, e) show the radii for the heavy atoms, while those in the right column (b, d, f) show the radii for the H/D atoms.

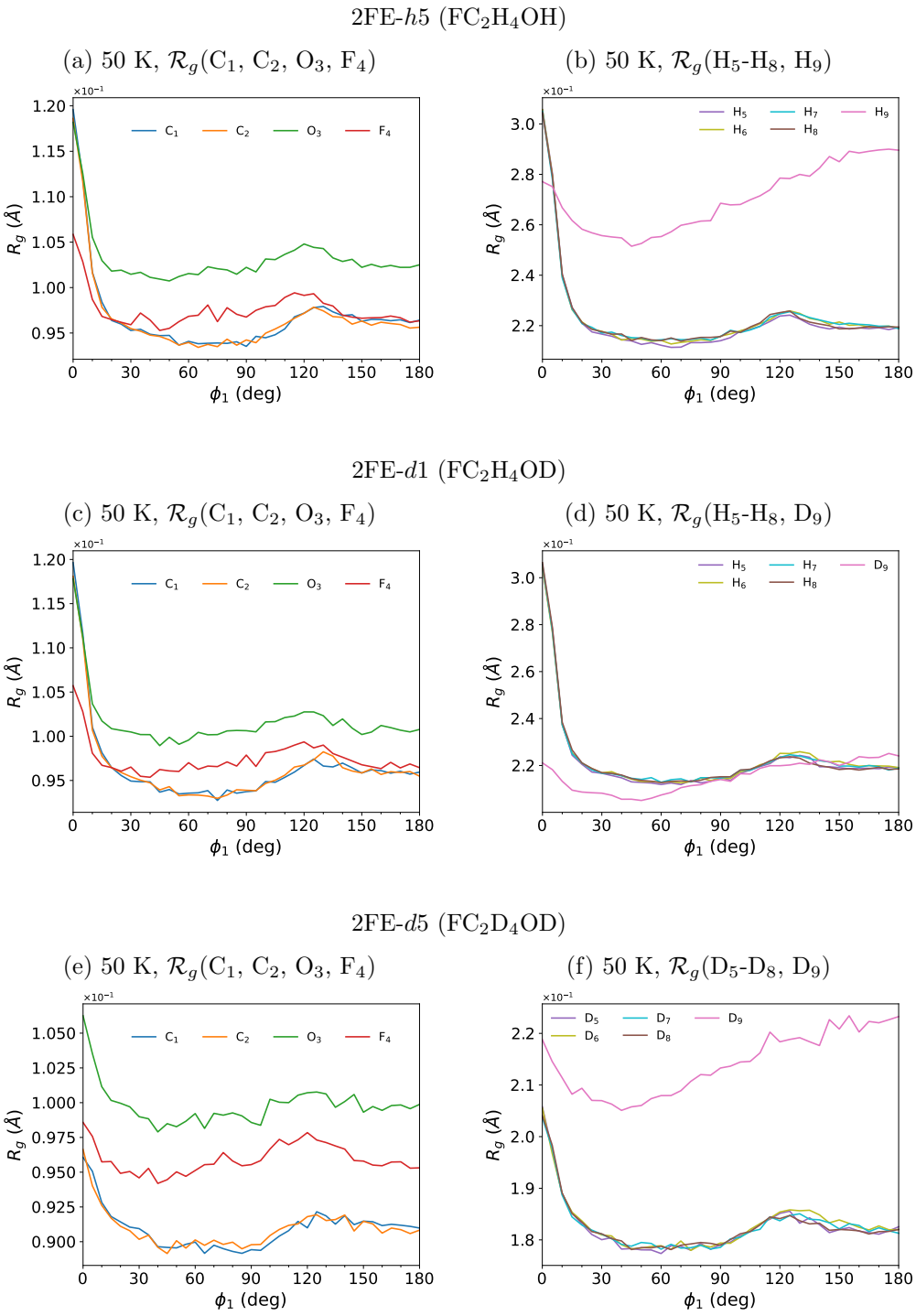

FIG. S-6. Radii of gyration, $\mathcal{R}_g$, for various atoms of 2FE from umbrella sampling simulations at 50 K as a function of the FCCO dihedral (ϕ_1). The top (a,b), middle (c,d) and bottom (e,f) rows provide the trends for 2FE-$h5$, 2FE-$d1$ and 2FE-$d5$, respectively. The plots in the left column (a, c, e) show the radii for the heavy atoms, while those in the right column (b, d, f) show the radii for the H/D atoms.

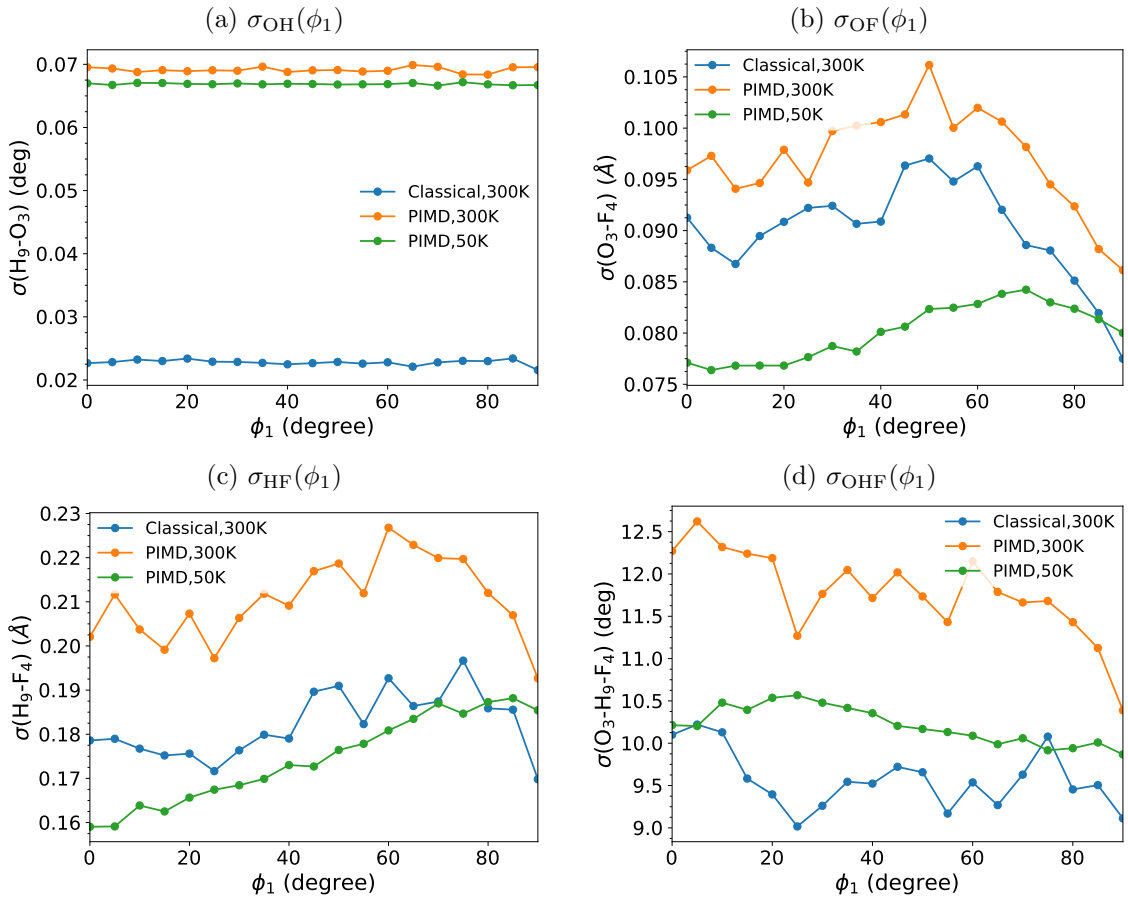

FIG. S-7. Widths of the distributions of the (a) OH, (b) OF and (c) HF distances and (d) the HOF angle as a function of ϕ_1 for geometries obtained from umbrella sampling. The corresponding trends of the averages are provided in the main text. For the analyses, only those geometries with $-120^\circ \leq \phi_2 \leq 0^\circ$ for $\phi_1 > 30^\circ$ and $-60^\circ \leq \phi_2 \leq 60^\circ$ for $\phi_1 < 30^\circ$ are considered; see Fig. S-4 for the (ϕ_1, ϕ_2) distributions.

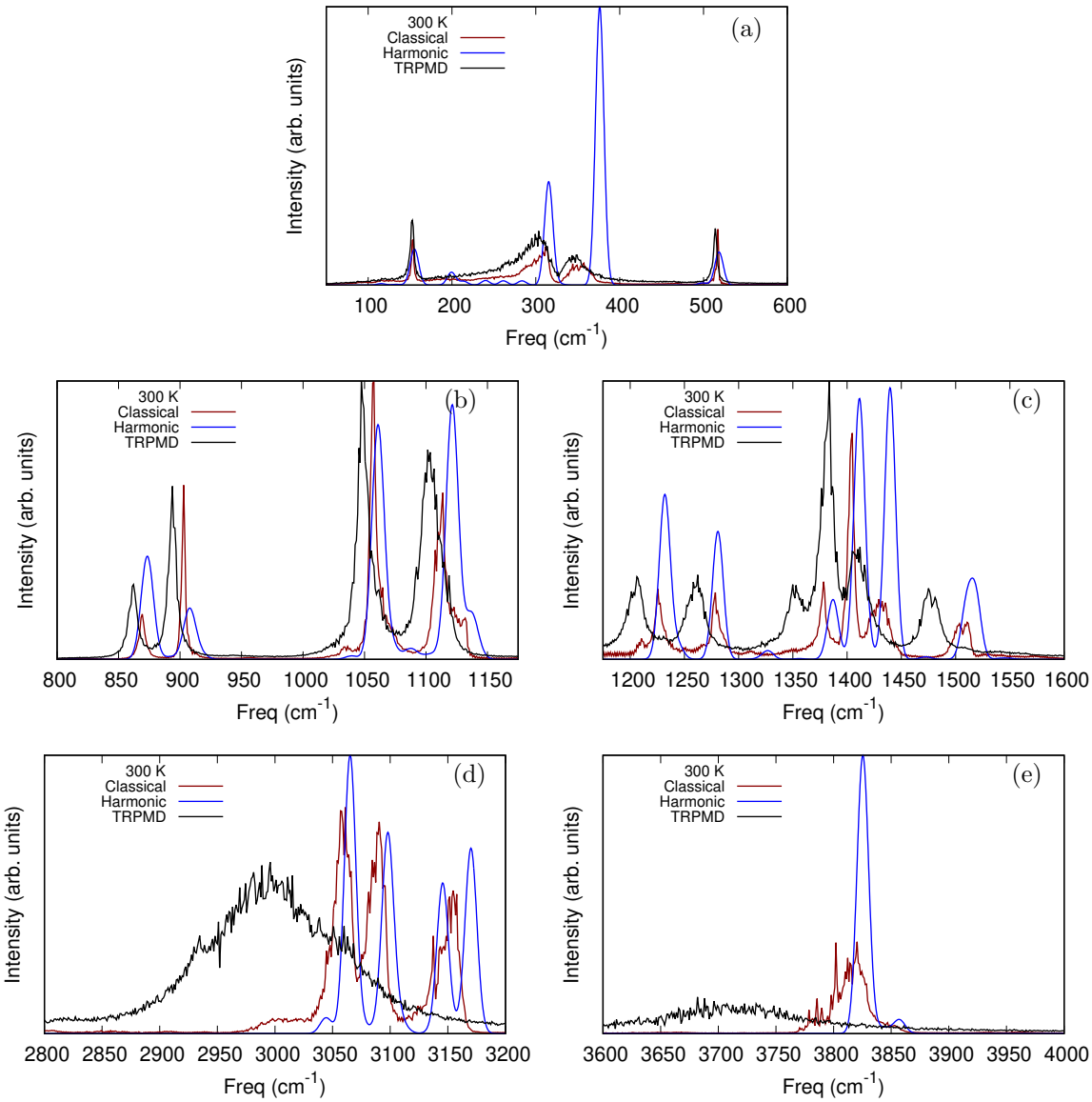

FIG. S-8. A comparison of the harmonic spectrum with those from classical and TRPMD simulations at 300 K. The spectra as plotted over ranges (a) 50–600 cm^{-1}, (b) 800–1175 cm^{-1}, (c) 1175–1600 cm^{-1}, (d) 2800–3200 cm^{-1}, (e) 3600–4000 cm^{-1}, for ease of comparison. The harmonic spectrum is generated from normal mode unscaled frequencies (Table S-2) and intensities. The latter is within the double harmonic approximation, taken directly from frequency calculations with Gaussian 16 at each minimum. A 5 cm^{-1} Gaussian is applied to each stick. In the final harmonic spectrum, each conformer is weighted by its Boltzmann population (based on the ab initio energy relative to the G^+g^- minimum) and degeneracy.

[1] S. E. Brown, *J. Chem. Phys.*, 2019, **151**, 194111.
[2] X. Huang, B. J. Braams and J. M. Bowman, *J. Chem. Phys.*, 2005, **122**, 044308.
[3] C. R. Harris, K. J. Millman, S. J. van der Walt, R. Gommers, P. Virtanen, D. Cournapeau, E. Wieser, J. Taylor, S. Berg, N. J. Smith, R. Kern, M. Picus, S. Hoyer, M. H. van Kerkwijk, M. Brett, A. Haldane, J. F. del Río, M. Wiebe, P. Peterson, P. Gérard-Marchant, K. Sheppard, T. Reddy, W. Weckesser, H. Abbasi, C. Gohlke and T. E. Oliphant, *Nature*, 2020, **585**, 357–362.